

BORON NITRIDE NANOTUBES



Mechanical characterization of electrospun boron nitride nanotube-reinforced polymer nanocomposite microfibers

Nasim Anjum¹, Ohood Q. Alsmairat², Zihan Liu¹, Cheol Park³, Catharine C. Fay³, Changhong Ke^{1,4,a)} 

¹Department of Mechanical Engineering, State University of New York at Binghamton, Binghamton, NY 13902, USA

²Department of Mechanical Engineering, University of Texas at Tyler, Tyler, TX 75799, USA

³Advanced Materials and Processing Branch, NASA Langley Research Center, Hampton, VA 23681, USA

⁴Materials Science and Engineering Program, State University of New York at Binghamton, Binghamton, NY 13902, USA

a) Address all correspondence to this author. e-mail: cke@binghamton.edu

Received: 13 April 2022; accepted: 6 July 2022

Boron nitride nanotubes (BNNTs) are promising fillers for reinforcing polymers toward lightweight and high-strength nanocomposite materials. Understanding the interfacial load transfer mechanism is of importance to take advantage of the extraordinary structural and mechanical properties of BNNTs. Here, we investigate the mechanical properties of electrospun BNNT-reinforced polymethyl methacrylate (PMMA) nanocomposite microfibers. The local load transfer on the BNNT-PMMA interface inside the nanocomposite microfiber is characterized based on in situ Raman micromechanical measurements. The effective interfacial shear strengths of 0.1%, 0.5%, and 0.65% BNNT-PMMA microfibers are found to be about 78.4 MPa, 60.9 MPa, and 50.7 MPa, respectively, which correspond to the increases of Young's modulus (tensile strength) of about 67% (25%), 108% (60%), and 133% (69%) from pure PMMA microfibers. The study reveals the constitutive role of the nanotube-polymer interfacial strength in the composite's mechanical property enhancement. The findings contribute to a better understanding of the process-structure-property relationship and the reinforcing mechanism of nanotube-based nanocomposites.

Introduction

The lightweight and high-strength characteristics of nanofiber-reinforced polymer nanocomposites hold promise for a number of applications that benefit a wide range of industries such as aerospace, automotive, and biomedical industries [1]. Boron nitride nanotubes (BNNTs) [2, 3] are a type of one-dimensional tubular structure composed of hexagonal lattice networks of covalent and partially ionic B-N bonds. BNNTs are a promising reinforcing nanofiller material because of their low density and superior structural and mechanical properties. BNNTs possess an elastic modulus of up to 1.3 TPa and a tensile strength of up to 33 GPa [4–13], which are on a par with carbon nanotubes (CNTs). Our recent studies reveal that BNNTs are superior to CNTs in reinforcing polymers because BNNTs can form much stronger binding interfaces with polymers than CNTs, thanks to their

highly polarized electronic structures [14]. In addition, BNNTs possess excellent resistance to oxidations [15, 16], remarkable characteristics of thermal conductivities [17], chemical inertness and electrical insulation [2, 18], as well as irradiation shielding [19]. Therefore, BNNT-reinforced polymer nanocomposites are promising multifunctional engineering materials for tackling some of the most demanding applications, such as the body of aerospace vehicles. In contrast to an extensive literature on CNT-based nanocomposites, the reported studies about BNNT-reinforced nanocomposites remain quite limited [20–24], which is, in part, due to the challenges in manufacturing high-quality BNNTs and the resulting limited availability of this material to the research community.

Generally, because the mechanical properties of nanotubes exceed those of polymers by two to three orders of magnitudes,

even a small addition could lead to a substantial property enhancement [25]. The envisioned property enhancement in nanotube-reinforced polymer nanocomposites is governed by the nanotube dispersion and alignment inside the matrix, the load transfer on the nanotube–matrix interface, and other factors. A nanotube's large surface-to-volume characteristics enable more interfacial contact with the matrix, which is advantageous to the interfacial load transfer and thus the bulk property enhancement. On the other hand, nanotubes are prone to aggregation caused by the strong inter-nanotube van der Waals interaction, which results in structural nonidealities, such as nanotube bundling and networking. Even for nanotubes in initially well-dispersed solutions, mixing with a polymer resin makes their structural conformation inside the composite far from the ideal, particularly at large nanotube concentrations. The resulting conformational nonidealities negatively influence both the nanotube alignment as well as the effective load transfer on the nanotube–matrix interface. Therefore, knowledge of how the nanotube alignment inside the matrix and the resulting effective load transfer characteristics influence the bulk property enhancement is essential to a complete understanding of the reinforcing mechanism and the optimal design and manufacturing of nanotube-reinforced nanocomposites.

In this work, we investigate the bulk and local mechanical properties of BNNT-reinforced polymethyl methacrylate (PMMA) nanocomposite microfibers and the constitutive relationship that governs the bulk composite properties enhancement. BNNT-PMMA microfibers were manufactured using electrospinning techniques. The microfiber was produced by ejecting a BNNT-PMMA solution from a syringe pipette with the electrostatic force generated from an externally applied voltage. The viscous force in liquid flow facilitates the nanotube alignment along the longitudinal direction of the microfiber. The alignment of nanotubes inside the composite microfiber was quantified using polarized Raman microscopy techniques [26]. In situ Raman micromechanical measurements were performed to quantify the mechanical loading of nanotubes inside the composite microfiber during tensile measurements. The effective interfacial shear strength (IFSS) of the BNNT–polymer interface was calculated based on the measured critical strain values that correspond to the collective slip on the nanotube–polymer interface and the overall nanotube alignment inside the composite microfiber. The research reveals that adding 0.1–0.65% of BNNTs in PMMA substantially enhances its bulk mechanical properties. The IFSS is found to decrease with nanotube loading and is well below the reported values obtained by single-nanotube pullout techniques. The comparison between micromechanics-based theoretical predictions of the bulk composite properties and experimental measurements reveals the constitutive role of the nanotube–polymer interfacial strength in the composite's mechanical property enhancement.

This work provides new insights into the nanotube reinforcing mechanism and the process–structure–property relationship of BNNT-reinforced nanocomposites that will be useful to fully exploit the potentials of BNNTs as reinforcing fillers for nanocomposite applications.

Results and discussion

Tensile measurements of electrospun PMMA and BNNT-PMMA microfibers

Figure 1(a) shows a piece of BNNT puffballs that were employed in the manufacturing of BNNT-PMMA composite microfibers. Typical electrospun BNNT-PMMA microfibers form a mesh structure on the collector as shown in Fig. 1(b, c). Through adjusting the electrospinning parameters, the diameter of microfibers can be widely tuned from sub-microns to a few hundreds of microns. For ease of handling, microfibers with diameters of 10–20 μm were chosen. Figure 1(d) shows the representative tensile testing curves of four microfibers with varying BNNT concentrations (i.e., 0%, 0.1%, 0.5%, and 0.65%). The displayed results show that the addition of BNNTs leads to a significant increase in Young's modulus and tensile strength, and the property enhancement increases with BNNT loading. Figure 1(e) shows the broken surface of one fractured 0.65% BNNT-PMMA microfiber with some nanotubes protruding from the polymer matrix, and the protruding nanotube lengths are measured to be from ~ 0.3 to ~ 1.2 μm . The protrusions resulted from the debonding of the nanotube–polymer interface during the tensile tests and indicate the effective load transfer on the nanotube–polymer interface, which accounts for the observed enhancement of the bulk mechanical properties of BNNT-PMMA microfibers. The strong van der Waals interactions cause some of the protruding nanotubes on the fractured surface to aggregate and bundle [Fig. 1(e) inset]. Figure 1(e) shows that the electrospun microfibers possess some degree of porosity, which weakens their mechanical properties.

The bulk mechanical properties of pure PMMA and BNNT-PMMA microfibers were obtained based on the tensile measurement of six different specimens for each type of microfibers. The results are shown in Fig. 1(f) and listed in Table 1. Young's modulus and tensile strength of PMMA microfibers are measured to be ~ 1.2 GPa and ~ 18 MPa, respectively. The addition of 0.1% BNNT increases Young's modulus and tensile strength of PMMA by about 67% and 25% to ~ 2.0 GPa and ~ 22.5 MPa, respectively. The addition of 0.5% and 0.65% BNNT increases Young's modulus (tensile strength) of PMMA by $\sim 108\%$ (60%) and $\sim 133\%$ (69%), respectively. The results clearly show that a tiny addition of BNNTs can lead to significant improvements to the bulk mechanical properties of polymers. The property enhancement is not linearly proportional to nanotube loading. The

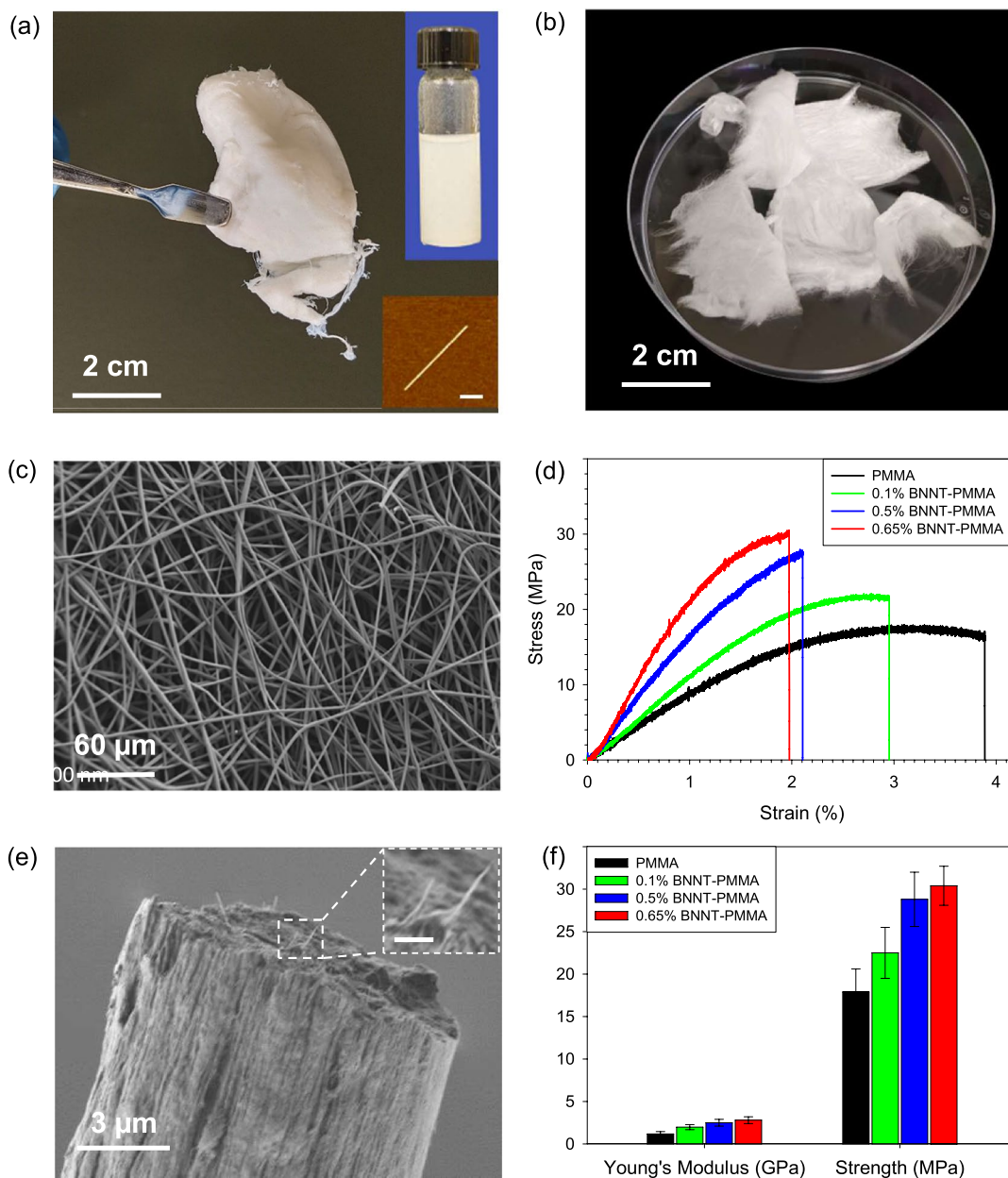


Figure 1: (a) A portion of the as-received BNNT puffballs (~16 mg) held by a tweezer; insets (*upper* dispersed BNNT solution; *lower* AFM image of a typical BNNT (~800 nm in length and ~3.2 nm in diameter, *scale bar* 200 nm); (b) Optical image and (c) SEM image of electrospun 0.1% BNNT-PMMA composite microfiber meshes; (d) Tensile testing results of one PMMA and three BNNT-PMMA composite microfibers with different nanotube concentrations. (e) SEM image of the fractured surface of one tested 0.65% BNNT-PMMA microfiber and a zoom-in view (*scale bar* 500 nm). (f) Comparisons of the mechanical properties of PMMA and BNNT-PMMA microfibers.

property enhancement of Young's modulus (tensile stress) on a per 0.1% BNNT basis for 0.1, 0.5, and 0.65% BNNT-PMMA composites is found to be about 67% (25%), 22% (12%), and 20% (11%), respectively. The property enhancement on a per-unit nanotube loading basis is the greatest at the lowest nanotube loading and decreases with an increase in nanotube loading.

In situ Raman micromechanical measurements

In situ Raman micromechanical measurements were conducted on individual electrospun BNNT-PMMA microfibers to better understand the local interfacial load transfer inside the composite microfiber. Figure 2(a) shows the comparison of the Raman spectra of BNNTs, and electrospun PMMA and BNNT-PMMA

TABLE 1: Summary of the experimentally measured and theoretically calculated/predicted parameters on the bulk mechanical properties and the interfacial shear strength of PMMA and BNNT-PMMA microfibers (ROM rule of mixtures; HT Halpin–Tsai).

Parameter	Methodology		PMMA	0.1% BNNT-PMMA	0.5% BNNT-PMMA	0.65% BNNT-PMMA
Young's modulus (GPa)	Experimental		1.2 ± 0.3	2.0 ± 0.3	2.5 ± 0.4	2.8 ± 0.4
	Predicted	ROM	–	1.6 ± 0.3	3.1 ± 0.6	3.7 ± 0.7
		HT	–	1.4 ± 0.3	2.4 ± 0.6	2.8 ± 0.6
Tensile strength (MPa)	Experimental		18 ± 2.7	22.5 ± 3.0	28.8 ± 3.2	30.4 ± 2.3
	Predicted (ROM)		–	21.8 ± 2.7	31.4 ± 3.0	32.1 ± 3.0
Critical strain (%)	Experimental		–	0.97 ± 0.15	0.68 ± 0.10	0.55 ± 0.08
Effective IFSS (MPa)	Calculated		–	78.4 ± 15.8	60.9 ± 11.9	50.7 ± 9.9

microfibers. BNNTs show a characteristic peak at $\sim 1369 \text{ cm}^{-1}$ [27, 28], which is attributed to its active E_{2g} mode. The peak frequency of this h-BN Raman band is sensitive to external strain that changes the B–N bond length. In comparison, the Raman spectrum of PMMA displays several characteristic bands, but no visible PMMA bands exist between the 1350 and 1377 cm^{-1} range. Therefore, the 1369 cm^{-1} peak is considered the fingerprint of BNNTs in the composite microfiber. The spectrum of one 0.65% BNNT-PMMA microfiber [red curve in Fig. 2(a)] shows a BNNT peak at $\sim 1368.5 \text{ cm}^{-1}$. The slight downshift ($\sim 0.5 \text{ cm}^{-1}$) of the BNNT peak indicates that the nanotubes in the composite were actually under tensile stress, which was likely introduced during the microfiber manufacturing and processing stages. The resulting elongation of the B–N bond leads to a bond softening and a lower Raman peak frequency. Figure 2(b) shows the selected in situ Raman spectra recorded for one tensile-stretched 0.1% BNNT-PMMA microfiber, which display a gradual downshift of the h-BN peak frequency from about 1367.5 cm^{-1} at zero strain to 1365.2 cm^{-1} at 1% strain. Then the peak shift remains little changed when the tensile strain increases to 1.9%. The continuous peak frequency downshift indicates that the nanotubes in the composite microfiber experience an increasing normal strain that results from the stress transferred through the nanotube–polymer interface. The little-changed peak frequency at large strains indicates strain (stress) saturation in the nanotubes. We conclude that the interfacial load transfer reaches a maximum limit, and the onset of slips occurs on the interface. Figure 2(c) shows the measured dependence of the h-BN peak frequency on strain for BNNT-PMMA microfibers at various BNNT loadings. All three curves display a similar trend that comprises two distinct segments: the peak frequency first downshifts nearly linearly with strain, then stays in a narrow band with further increases of strain, the latter of which indicate the saturation of the load transfer at the nanotube–polymer interface. The strain at the joint of these two segments is considered to correspond to the onset of the collective slip on the nanotube–polymer interface and is named “critical strain” here. The critical strain is found to be $\sim 0.97\%$ for 0.1%, $\sim 0.68\%$ for 0.5%, and $\sim 0.55\%$ for 0.65% BNNT-PMMA

microfibers, which are shown in Fig. 2(d). The decrease of the critical strain indicates a smaller load transferred via the composite interface at higher nanotube loadings, which is consistent with the aforementioned observation that the per-unit nanotube loading-based bulk property enhancement decreases with an increase in nanotube loading.

Polarized Raman microscopy measurements

The nanotube alignment inside the composite is an essential parameter in the quantitative understanding of the nanotube reinforcement and the bulk and local mechanical properties of nanotube-reinforced nanocomposites. The electrospinning technique facilitates the nanotube alignment along the longitudinal direction of the microfiber via the viscous force–nanotube interaction during the solution ejection process. Here, polarized Raman microscopy (PRM) measurements were conducted to characterize the overall alignment of BNNTs inside the composite microfiber. PRM techniques [29] use the one-dimensional characteristics of nanotubes and the dependence of the nanotube's Raman scattering intensity on the nanotube's orientation angle to the incident polarized laser beam, as shown in Fig. 3(a). The Raman signal is strongest when the polarization of the incident laser beam is parallel to the nanotube's longitudinal axis and weakest along the nanotube's transverse (radial) direction. Figure 3(b) shows selected PRM spectra for a 0.5% BNNT-PMMA microfiber. The h-BN peak intensity decreases monotonously as the microfiber orientation angle increases from 0° to 90° , which is consistently exhibited in the PRM measurements on three typical BNNT-PMMA microfibers with various nanotube loadings [Fig. 3(c)]. The maximum Raman peak intensity reduction is found to be about 60% (0.1%), 70% (0.5%), and 75% (0.65%). The remarkable Raman peak intensity reduction indicates that the nanotubes inside the composite microfiber are preferably oriented along the microfiber's longitudinal direction. The overall orientation angle of the nanotubes inside the composite is calculated by interpreting the PRM measurements using the model reported by Gorman

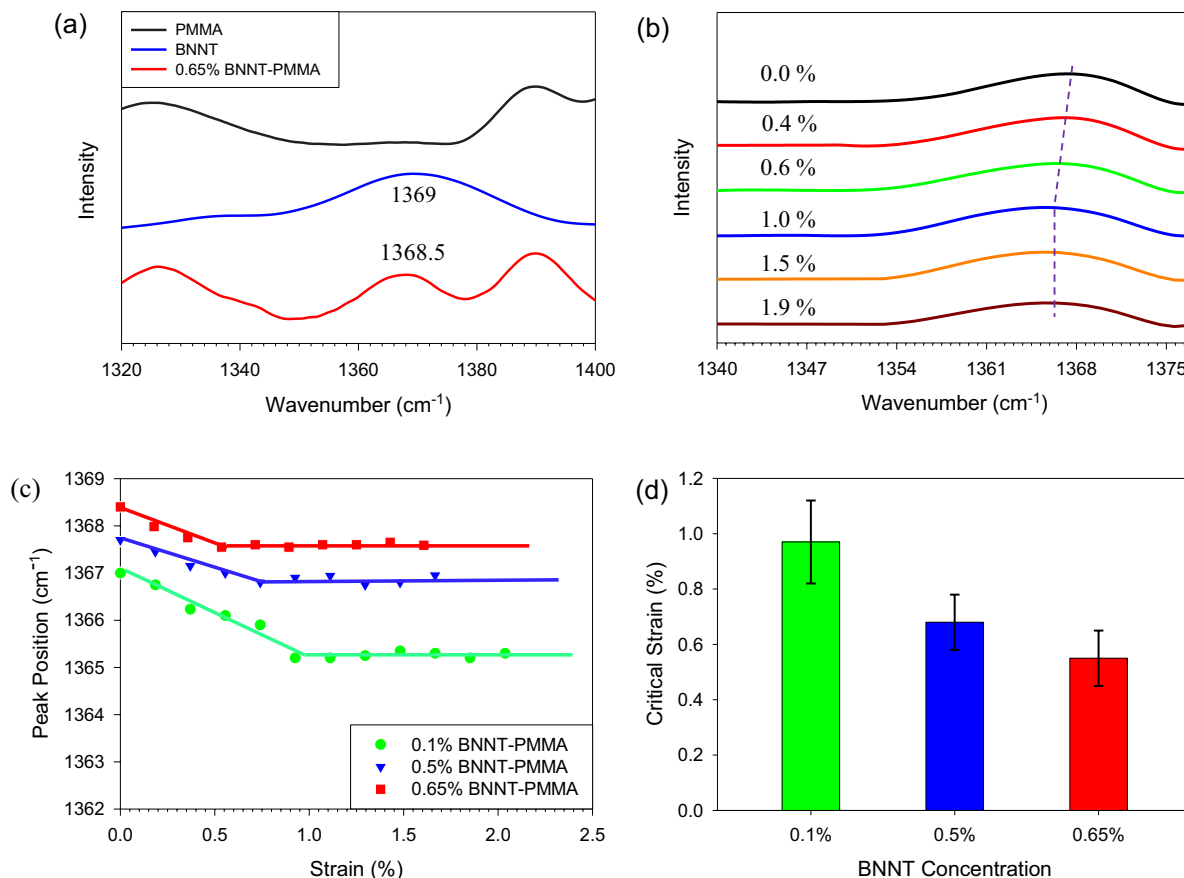


Figure 2: (a) Typical Raman spectra of PMMA, BNNTs, and 0.65% BNNT-PMMA microfibers. (b) Selected Raman spectra of a 0.1% BNNT-PMMA microfiber at different tensile strains. The dashed line indicates the trend of the BNNT peak intensity change. (c) The measured dependence of the BNNT peak intensity on the tensile strain for individual BNNT-PMMA microfibers. The solid curves are the bi-linear fitting lines to the respective measurement data. (d) The measured critical strain for BNNT-PMMA microfibers at various nanotube concentrations.

et al. [29], in which the nanotube's characteristic Raman peak intensity (I) is given as

$$I(\varphi) \propto p \int_{\varphi-\alpha}^{\varphi+\alpha} \cos^4(\varphi) d\varphi + (1-p) \int_{\varphi+\alpha}^{\pi+\varphi-\alpha} \cos^4(\varphi) d\varphi, \quad (1)$$

where φ is the angle of the composite microfiber's axis with respect to the incident polarized light, α is the angle of a nanotube's axis with respect to the microfiber's axis, and p is the mole fraction of the nanotubes whose axes are within $\pm \alpha$ of the microfiber's axis. The values of p and α are obtained through curve fitting the PRM measurement as shown in Fig. 3(c) using Eq. 1, and the results are summarized in Table 2. Our analysis shows that the measured Raman peak intensity data can be well-fitted using Eq. 1 with a p value within the range of 88.5–91%, and the corresponding α values are found to be $\sim 5.6^\circ$ for 0.1%, $\sim 10.5^\circ$ for 0.5%, and $\sim 13.5^\circ$ for 0.65% BNNT-PMMA microfibers, respectively. The results confirm that the

electrospinning process facilitates the nanotube alignment inside the manufactured composite microfiber. A large majority of the nanotubes orient within a reasonably small angle from the composite microfiber's axis, and noticeably better nanotube alignment occurs in the composite microfibers with lower nanotube loadings, the latter of which can be attributed to weaker inter-nanotube interactions as a result of the statistically larger inter-nanotube spacing.

Micromechanics calculations of the interfacial shear strength

We investigate the local mechanical properties of BNNT-PMMA composites based on the bulk mechanical characterization and in situ Raman and polarized Raman measurements. As shown in Fig. 4(a), a simplified micromechanics model is established to quantify the interfacial load transfer inside the composite microfiber. Several assumptions are made in this equivalent composite

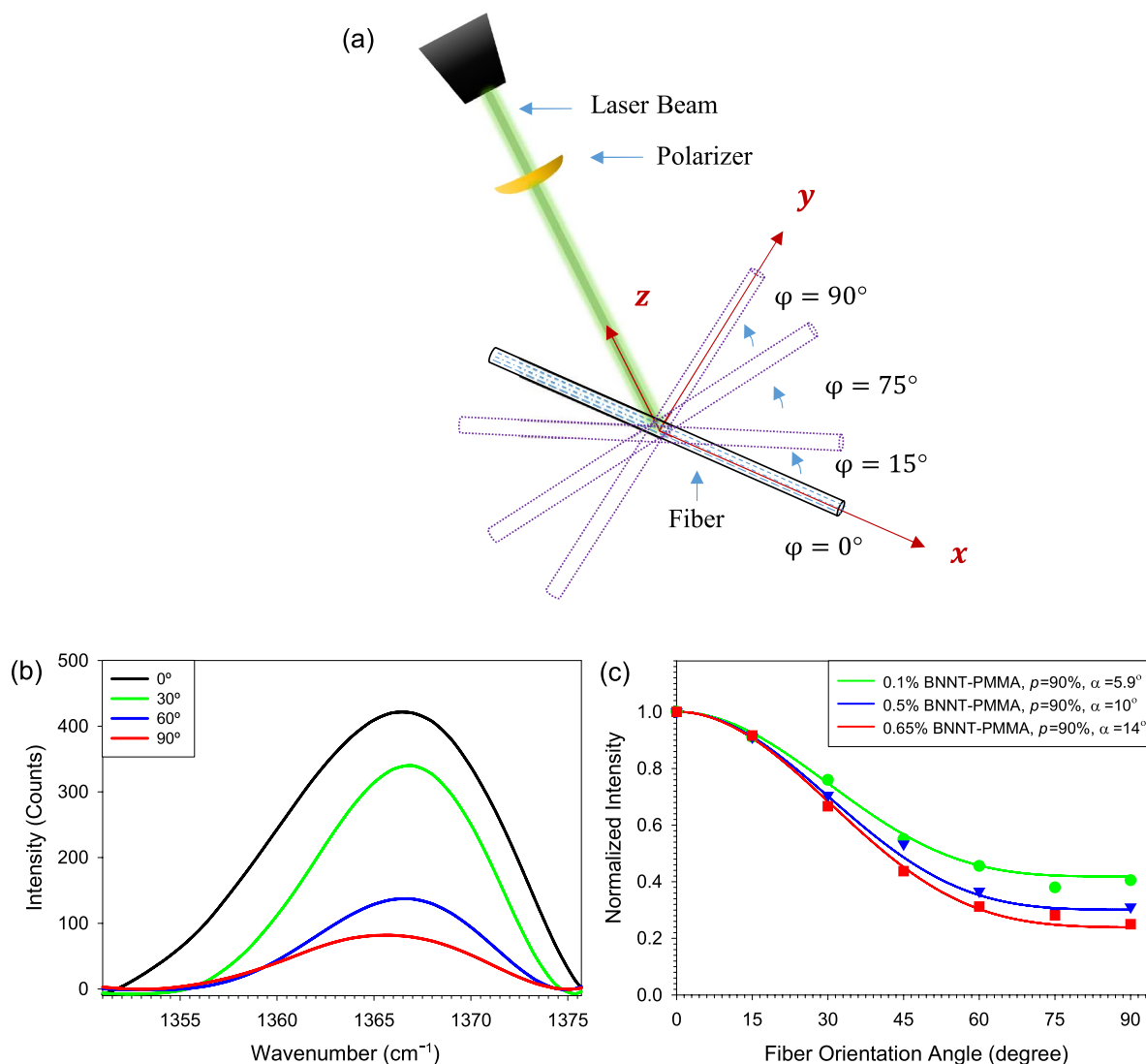


Figure 3: (a) Schematic of the experimental setup of the polarized Raman measurement. (b) Polarized Raman spectra of a 0.5% BNNT-PMMA microfiber at selected microfiber orientation angles. (c) The measured dependence of the BNNT peak intensity on the microfiber orientation angle. The solid curves are the respective fitting curves obtained based on Eq. 1.

system to the experimentally tested electrospun nanotube composite microfiber: (i) all the nanotubes in the composite are straight and uniformly distributed across the cylinder-shaped composite and undertake the same orientation angle α from the composite's longitudinal axis. (ii) The inter-nanotube interactions are neglected because of relatively low nanotube loadings. The interfacial load transfer on the nanotube–matrix interface reportedly follows a shear lag effect [30]. The maximum interfacial shear stress (i.e., IFSS) occurs at the nanotube entry and exit positions and decays toward the center of the nanotube [Fig. 4(b)]. For a sufficiently long nanotube, the interfacial shear stress in the central portion of the nanotube is close to zero. The central portion of the nanotube has the same deformation

(i.e., normal strain) as in the surrounding matrix. The interfacial shear stress distribution on the nanotube surface is given as [26]

$$\tau = \frac{E_{nt}\epsilon \cos^2 \alpha \cdot n \cos h(2n \cdot x/D_{nt})}{2 \sin h(n \cdot l/D_{nt})}, \quad (2)$$

where x is the coordinate along the nanotube's longitudinal direction, l is the nanotube length, ϵ is the normal strain in the central portion of the nanotube, E_{nt} is the nanotube's Young's modulus, $n = \sqrt{\frac{E_m}{E_{nt} \cdot (1 + \nu_m) \cdot \log(D_m/D_{nt})}}$, in which E_m and ν_m are the matrix's Young's modulus and Poisson's ratio, respectively. The interfacial shear stress reaches the maximum value at $x = \pm l/2$ when the strain inside the central portion of the nanotube reaches the critical value (ϵ_{cr}) that corresponds to the onset of the collective interfacial slip and is given as

$\tau_{\max} = \frac{E_m \epsilon_{cr} \cos^2 \alpha \cdot n}{2 \cdot \tanh(n \cdot l / D_{nt})} \cdot \tau_{\max}$ is calculated to be about 78.4 ± 15.8 MPa (0.1%), 60.9 ± 11.91 MPa (0.5%), and 50.7 ± 9.9 MPa (0.65%). The calculations are based on the following parameters: $E_m = 1.2 \pm 0.3$ GPa; $\nu_m = 0.32$ [31]; $D_{nt} = 2.9$ nm; $E_{nt} = 1.07 \pm 0.11$ TPa [12] and $l = 1000$ nm (τ_{\max} is found independent of l when $l > 872$ nm for nanotube loadings studied in this work considering a threshold shear stress of 1 MPa); the diameter of the cylindrical matrix $D_m = 105$ nm (0.1%), 47 nm (0.5%), and 36 nm (0.65%) that are calculated based on the densities of PMMA (1.18 g/cm³) and BNNTs (1.35 g/cm³). The lower effective IFSS in composite microfiber with higher nanotube loadings indicates that the nanotubes undertake smaller loads, which is plausibly the reason (or at least one major reason) accounting for the under-proportional increase of the bulk mechanical properties. The pointwise interfacial shear stress distribution characteristics corresponding to the initiation of the interfacial slip are shown in Fig. 4(c). The correlations among the results of the IFSS, the nanotube alignment, and the critical strain show that a better nanotube alignment inside the composite leads to a larger critical strain, and these two factors result in a more effective interfacial load transfer [23].

The mechanical strength of BNNT-PMMA interfaces was previously characterized using an in situ SEM nanomechanical single-nanotube pullout technique [14]. In such a single-nanotube pullout experiment, a single straight BNNT partially embedded into a PMMA matrix is stretched out using a pre-calibrated atomic force microscopy cantilever. The tested interface is formed between the single nanotube and the matrix and is free of nonidealities produced from manufacturing and processing, such as nanotube bundling and networks, which often ubiquitously exist in bulk nanotube composites. The reported mechanical strength of this close-to-ideal BNNT-PMMA interface (~219 MPa) is significantly higher than the values (~50.7–78.4 MPa) obtained in this study. The low effective interfacial load transfer in the tested BNNT composite microfibers dwindles the reinforcing efficiency of strong nanotube fillers. Our analysis shows that the single-nanotube pullout value of

IFSS corresponds to a much higher critical strain ϵ_{cr} , i.e., 2.68% (0.1%), 2.36% (0.5%), and 2.25% (0.65%). The quantitative data about the effective interfacial load transfer in bulk BNNT-reinforced polymer nanocomposites provide insights into how and why nanotube loading affects the bulk mechanical properties of nanotube-reinforced nanocomposites.

Micromechanics predictions of the bulk mechanical properties of BNNT-polymer nanocomposites

Here, we use the micromechanics models to analyze and theoretically predict the bulk mechanical properties, specifically Young's modulus and tensile strength of the BNNT-PMMA composite and compare them to experimental measurements. We first analyze the following three possible failure scenarios of the composite: fracture of the matrix, fracture of nanotubes, and interfacial failure (slip). Because the measured tensile strain that corresponds to interfacial failure (0.55–0.97%) is lower than the measured ultimate strain of PMMA (~3%) and the reported ultimate strain of BNNTs (~1–3%), interfacial failure is considered to occur before the fracture of the matrix or nanotubes. We use the rule of mixtures (ROM) model and the Halpin-Tsai (HT) model to predict Young's modulus of the composite, while using the ROM model to predict its tensile strength.

Prediction of Young's modulus

- (a) *Rule of mixtures (ROM) model* Young's modulus of the composite is given as $E_c = [V_{nt} E_{nt}^e + (1 - V_{nt}) E_m]$, in which V_{nt} is the nanotube's volume ratio. E_{nt}^e is the effective modulus of the nanotube and is given by $E_{nt}^e = \frac{(D_{nt}^2 - D_{nt}^2 - inner)}{D_{nt}^2} E_{nt}$, in which $D_{nt} - inner$ is the nanotube's inner diameter. The usage of E_{nt}^e , in replace of E_{nt} , is justified because BNNTs are of a hollow tubular structure, and only the tubular shells contribute to load-bearing. For double-walled BNNTs, the median inner diameter is calculated to be 2.22 nm by consider-

TABLE 2: Summary of the nanotube alignment measurements of BNNT-PMMA microfibers using polarized Raman spectroscopy techniques.

Sample no.	0.1% BNNT-PMMA		0.5% BNNT-PMMA		0.65% BNNT-PMMA	
	ρ (%)	α (°)	ρ (%)	α (°)	ρ (%)	α (°)
1	90	5.3	90.5	12.5	88.5	12.5
2	91	5.8	88.5	10.0	90	14.0
3	89.8	6.3	89	11.0	89	15.0
4	90	5.9	90.1	9.5	90	14.1
5	90	5.3	89.2	10.2	89	12.0
6	91	5.0	90	10.0	89.5	13.5
Average and RMS value		5.6 ± 0.5		10.5 ± 1.0		13.5 ± 1.1

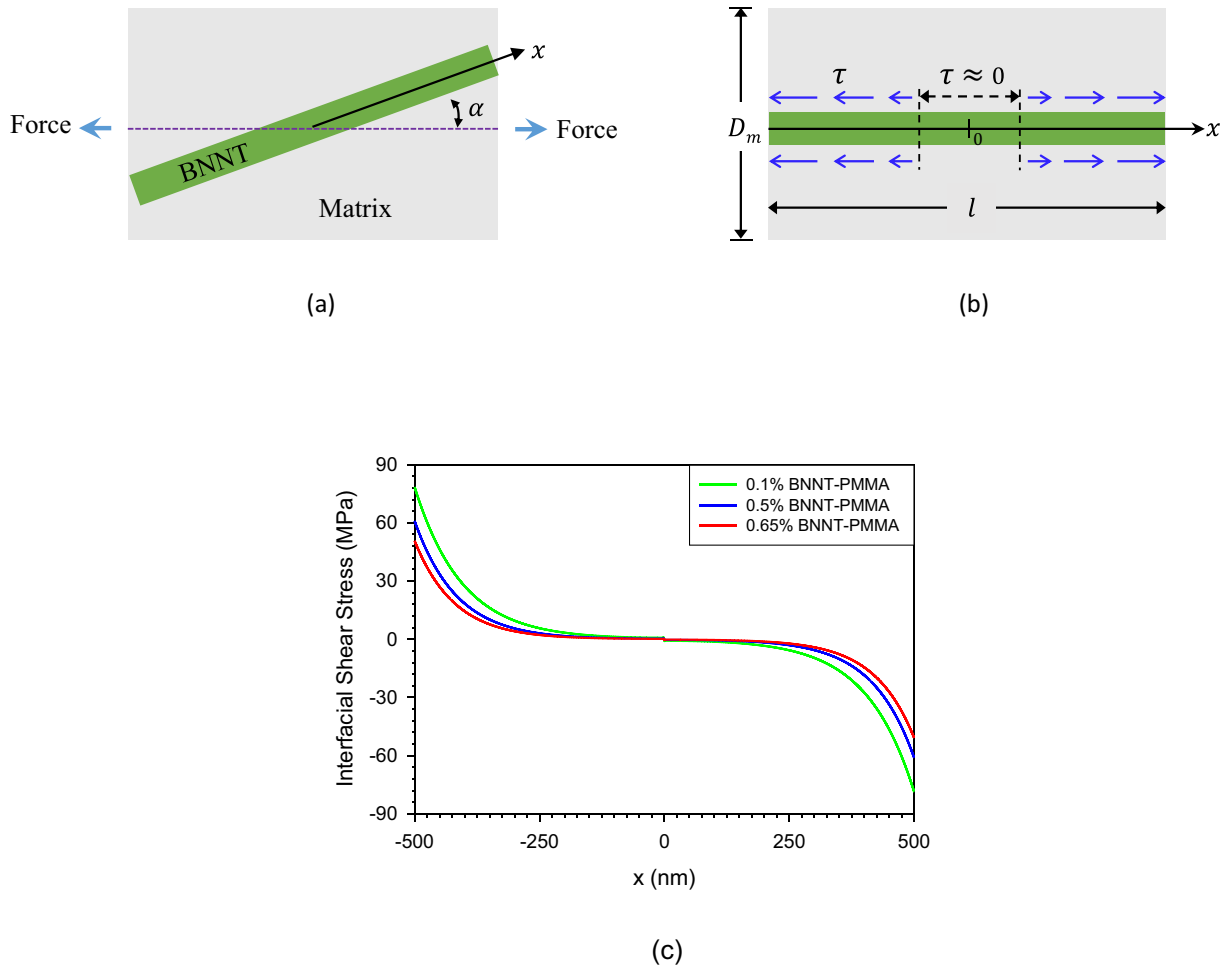


Figure 4: (a) Schematic of a single-nanotube composite in which the nanotube orients with an angle of α to the tensile force direction. (b) Schematic of the interfacial shear stress distribution on the surface of the nanotube that is concentrically embedded inside a same-length cylindrical polymer matrix. The blue arrows indicate the direction and magnitude of the interfacial shear stress. (c) The calculated interfacial shear stress distribution profiles at the respective critical strains for BNNT-PMMA microfibers with various nanotube loadings.

ing an interlayer BN distance of 0.34 nm, and E_{nt}^e is calculated to be about 454 ± 46 GPa. This model, as well as other models in this section, assumes a perfect nanotube alignment inside the composite microfiber (i.e., $\alpha = 0^\circ$).

- (b) *Halpin-Tsai (HT) model* Young's modulus of the composite is given as [32]

$$E_c = E_m \left(\frac{1 + \frac{2l}{D_{nt}} \eta V_{nt}}{1 - \eta V_{nt}} \right), \quad (3)$$

where the parameter η is given as $\eta = \frac{E_{nt}^e/E_m - 1}{E_{nt}^e/E_m + 2l/D_{nt}}$.

Figure 5(a) shows the theoretical predictions of Young's modulus of the BNNT-PMMA composite based on these two micromechanics models and the comparison with

experimental measurements, which are also listed in Table 1. For the 0.1% composite microfiber, the ROM-predicted Young's modulus (1.6 ± 0.3 GPa) is closer to the experimental measurement (2.0 ± 0.3 GPa) as compared to the HT-predicted value (1.4 ± 0.3 GPa). Nonetheless, the mean experimental value is noticeably higher than both predicted values. For the composite microfibers with 0.5% and 0.65% nanotube loadings, the HT-predicted Young's moduli (~ 2.4 GPa and ~ 2.8 GPa) are in good agreement with the respective experimental values (~ 2.5 GPa and ~ 2.8 GPa), while the ROM model predicts much larger values (~ 3.1 GPa and ~ 3.7 GPa). We want to highlight that the prior studies report that the added nanotubes are actively involved in polymerization in the vicinity of the nanotube-polymer interface in the CNT-reinforced PMMA composite [33], which likely leads to preferred polymer chain alignments and increases the mechanical properties of nanocomposites. Because BNNTs have stronger binding

interactions with PMMA than CNTs [14], such effects on polymer chains are expected to occur in BNNT-PMMA composites and could lead to a higher measured Young's modulus than theoretical predictions (0.1 wt%). The results further emphasize the relevance of superior nanotube-polymer interfacial interactions to bulk composite properties, which may lead to property enhancements that reach or exceed theoretical predictions.

Prediction of the tensile strength

Interfacial failure occurs before the fracture of the matrix and the nanotube. Once interfacial slip initiates, the load is transferred to the nanotube and the resulting stress/strain in the nanotube reach saturated values, which is consistent with in situ Raman micromechanical measurements. The stress in the matrix can still increase up to its tensile strength σ_m . Based on the rule of mixtures, the tensile strength of the composite is given as

$$\sigma_c = V_{nt} E_{nt}^c \epsilon_{cr} + (1 - V_{nt}) \sigma_m. \quad (4)$$

Figure 5(b) shows the predicted tensile strengths of the BNNT-PMMA composite microfibers using Eq. 4 and the comparison with experimental measurements. The predicted tensile strengths ~ 21.8 MPa (0.1%), ~ 31.4 MPa (0.5%), and ~ 32.1 MPa (0.65%) agree reasonably well with the experimentally measured values. Equation 4 shows that the critical strain ϵ_{cr} plays an important role in governing the tensile strength of the composite. The tensile strength of the BNNT-PMMA composite could be further improved substantially through maximizing the interfacial load transfer by means of employing better materials processing and manufacturing techniques. For example, for 0.65% BNNT-PMMA composite microfibers, assuming that the critical strain ϵ_{cr} reaches the value corresponding to the single-nanotube pullout IFSS (i.e., $\epsilon_{cr} = 2.25\%$) and keeping all other parameters intact, the predicted tensile strength (~ 76.0 MPa) exceeds the reported experimental value in this study (~ 30.4 MPa) by about 150% and is over a fourfold increase as compared to pure PMMA microfibers (~ 18 MPa). The findings highlight the importance of exploiting the synergy of nanocomposite manufacturing in enhancing the interfacial load transfer to maximize the bulk property performance of nanotube-reinforced nanocomposites.

Conclusion

In this paper, the bulk and local mechanical properties of electrospun BNNT-PMMA nanocomposite microfibers are investigated. The study shows that a small fraction of BNNTs can mechanically enhance the polymer, which is attributed to an effective interfacial load transfer on the nanotube-polymer

interface and a decent nanotube alignment inside the composite microfiber. The study reveals that interfacial load transfer in the bulk nanotube-reinforced polymer nanocomposite is more effective at a lower nanotube loading. Nonetheless, the measured interfacial shear strength remains well below the value obtained from single-nanotube pullout experiments performed on the close-to-ideal nanotube-polymer interface. The comparison between micromechanics-predicted bulk composite properties and experimental measurements reveals the prominent role of the nanotube-polymer interface in bulk property enhancement that may reach or exceed theoretical predictions. The findings further demonstrate that BNNTs are a promising reinforcing filler for polymer nanocomposites and contribute to a complete understanding of the process-structure-property relationship and the reinforcing mechanism of nanotube-based nanocomposites.

Materials and methods

The employed BNNTs were synthesized using a high temperature/pressure (HTP) method [34] and purchased from BNNT materials. The as-received BNNT materials were in the form of dry white puffballs [Fig. 1(a)] with an h-BN purity $> 99\%$ based on the manufacturer's datasheet. HTP-BNNTs reportedly possess a length of up to a few hundred microns and are mostly double-walled with a polydispersed diameter of 1–6 nm and a median diameter of about 2.9 nm [14, 35]. The BNNT-PMMA composite microfibers were manufactured by first dispersing BNNTs in a mixture of dimethylformamide (DMF) and acetone (1:1 weight ratio) at about 0.4–2.6 mg/ml using ultrasonication for 2 h [Fig. 1(a) upper inset]. The typical lengths of the dispersed nanotubes are found within a few hundred nm to a few microns by atomic force microscopic (AFM) imaging, as exemplified by the nanotube shown in Fig. 1(a) lower inset. PMMA (120,000 in molecular weight purchased from Sigma-Aldrich) was added into the dispersed BNNT solution or the mixed DMF/acetone solvent at a weight concentration of about 32%. The mixture was stirred at room temperature to achieve a uniform solution. PMMA and BNNT-PMMA microfibers were manufactured using a customized in-house built electrospinning setup with an Acopian power supply (5 kV), 18-gauge blunt-tip stainless steel needles, and a grounded aluminum sheet as the target (collector) that was placed at a distance of 16 cm from the needle tip. After manufacturing, microfibers were dried at 70 °C inside a vacuum oven for 12 h before measurements. Composite microfibers with three BNNT weight concentrations of 0.1%, 0.5%, and 0.65% were manufactured. Unless specified otherwise, all nanotube loading values in this paper refer to weight concentration.

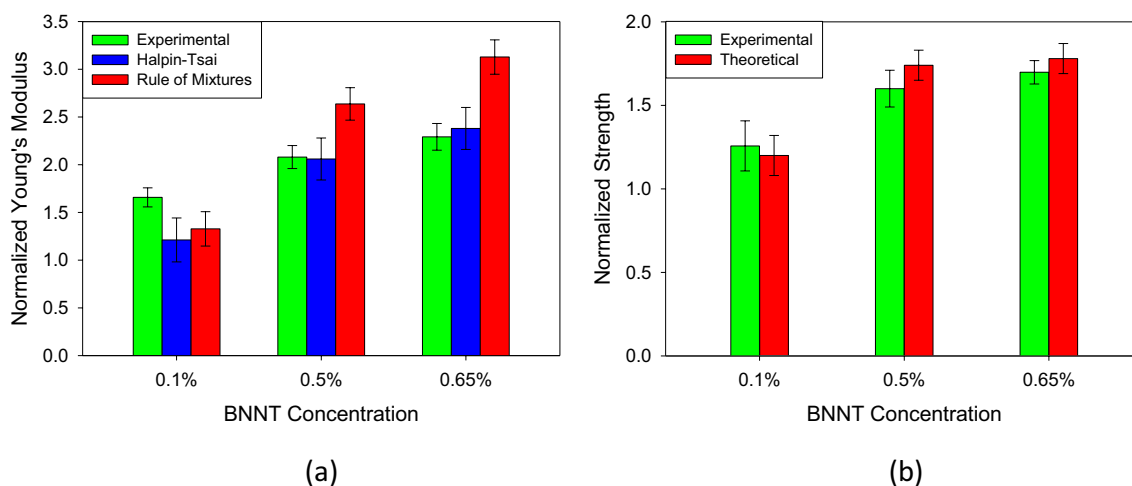


Figure 5: Comparison of the experimental measurements and theoretical predictions for (a) Young's modulus and (b) tensile strength of the BNNT-PMMA microfibers. All data are normalized with the respective mean values of PMMA microfibers.

Tensile measurements of PMMA or BNNT-PMMA microfibers with diameters of about 10–20 μm were performed using a universal tensile tester from ADMET with a 5 N load cell, a gauge length of about 6 mm, and a strain rate of 1 $\mu\text{m/s}$. In situ Raman micromechanical measurements were conducted using a Linkam tensile tester with a 20 N load cell and a strain rate of 1 $\mu\text{m/s}$ and a Renishaw inVia Raman microscope with a 532 nm laser and a 20 \times objective lens. The Raman spectra were acquired, in situ, at each 0.1% tensile strain mark. Polarized Raman spectroscopy measurements were conducted inside the Renishaw microscope with a polarizer, a 785 nm laser, and a 100 \times objective lens. A Zeiss scanning electron microscope (SEM) was used to image microfibers and the fracture surface of composite microfibers. An XE-70 AFM from Park Systems was used to image the dispersed BNNTs on silicon substrates.

Acknowledgments

This work was financially supported by the National Science Foundation under Grant No. CMMI-2009134 and the United States Air Force Office of Scientific Research under Grant No. FA9550-15-1-0491. The Raman spectroscopy measurements were performed using a facility acquired through an NSF-MRI Award (CMMI-1429176).

Funding

This work was financially supported by the National Science Foundation under Grant No. CMMI-2009134 and the United States Air Force Office of Scientific Research under Grant No. FA9550-15-1-0491. The Raman spectroscopy measurements

were performed using a facility acquired through an NSF-MRI Award (CMMI-1429176).

Data availability

The reported materials and data are available upon request.

Code availability

Not applicable.

Declarations

Conflict of interest The authors declare that they have no conflict of interest.

References

1. J. Baur, E. Silverman, Challenges and opportunities in multi-functional nanocomposite structures for aerospace applications. *MRS Bull.* **32**, 328–334 (2011)
2. A. Rubio, J.L. Corkill, M.L. Cohen, Theory of graphitic boron-nitride nanotubes. *Phys. Rev. B* **49**, 5081–5084 (1994)
3. N.G. Chopra, R.J. Luyken, K. Cherrey, V.H. Crespi, M.L. Cohen, S.G. Louie, A. Zettl, Boron-nitride nanotubes. *Science* **269**, 966–967 (1995)
4. M.M.J. Treacy, T.W. Ebbesen, J.M. Gibson, Exceptionally high Young's modulus observed for individual carbon nanotubes. *Nature* **381**, 678–680 (1996)
5. N.G. Chopra, A. Zettl, Measurement of the elastic modulus of a multi-wall boron nitride nanotube. *Solid State Commun.* **105**, 297–300 (1998)
6. R. Arenal, M.-S. Wang, Z. Xu, A. Loiseau, D. Golberg, Young modulus, mechanical and electrical properties of isolated

- individual and bundled single-walled boron nitride nanotubes. *Nanotechnology* **22**, 265704 (2011)
7. E. Hernandez, C. Goze, P. Bernier, A. Rubio, Elastic properties of C and B_xC_yN_z composite nanotubes. *Phys. Rev. Lett.* **80**, 4502–4505 (1998)
 8. H.M. Ghassemi, C.H. Lee, Y.K. Yap, R.S. Yassar, Real-time fracture detection of individual boron nitride nanotubes in severe cyclic deformation processes. *J. Appl. Phys.* **108**, 024314 (2010)
 9. D.-M. Tang, C.-L. Ren, X. Wei, M.-S. Wang, C. Liu, Y. Bando, D. Golberg, Mechanical properties of bamboo-like boron nitride nanotubes by in situ TEM and MD simulations: strengthening effect of interlocked joint interfaces. *ACS Nano* **5**, 7362–7368 (2011)
 10. A.P. Suryavanshi, M.-F. Yu, J. Wen, C. Tang, Y. Bando, Elastic modulus and resonance behavior of boron nitride nanotubes. *Appl. Phys. Lett.* **84**, 2527–2529 (2004)
 11. D. Golberg, P.M.F.J. Costa, O. Lourie, M. Mitome, X. Bai, K. Kurashima, C. Zhi, C. Tang, Y. Bando, Direct force measurements and kinking under elastic deformation of individual multiwalled boron nitride nanotubes. *Nano Lett.* **7**, 2146–2151 (2007)
 12. Y. Zhao, X. Chen, C. Park, C.C. Fay, S. Stupkiewicz, C. Ke, Mechanical deformations of boron nitride nanotubes in crossed junctions. *J. Appl. Phys.* **115**, 164305 (2014)
 13. M. Zheng, X. Chen, C. Park, C.C. Fay, N.M. Pugno, C. Ke, Nano-mechanical cutting of boron nitride nanotubes by atomic force microscopy. *Nanotechnology* **24**, 505719 (2013)
 14. X. Chen, L. Zhang, C. Park, C.C. Fay, X. Wang, C. Ke, Mechanical strength of boron nitride nanotube-polymer interfaces. *Appl. Phys. Lett.* **107**, 253105 (2015)
 15. Z. Xu, D. Golberg, Y. Bando, Electrical field-assisted thermal decomposition of boron nitride nanotube: experiments and first principle calculations. *Chem. Phys. Lett.* **480**, 110–112 (2009)
 16. X. Chen, C.M. Dmuchowski, C. Park, C.C. Fay, C. Ke, Quantitative characterization of structural and mechanical properties of boron nitride nanotubes in high temperature environments. *Sci. Rep.* **7**, 1–9 (2017)
 17. Y. Xiao, X.H. Yan, J.X. Cao, J.W. Ding, Y.L. Mao, J. Xiang, Specific heat and quantized thermal conductance of single-walled boron nitride nanotubes. *Phys. Rev. B* **69**, 205415 (2004)
 18. X. Blase, A. Rubio, S.G. Louie, M.L. Cohen, Stability and band gap constancy of boron nitride nanotubes. *EPL* **28**, 335 (1994)
 19. S.A. Thibeault, J.H. Kang, G. Sauti, C. Park, C.C. Fay, G.C. King, Nanomaterials for radiation shielding. *MRS Bull.* **40**, 836–841 (2015)
 20. W. Wang, Z. Li, E. Prestat, T. Hashimoto, J. Guan, K.S. Kim, C.T. Kingston, B. Simard, R.J. Young, Reinforcement of polymer-based nanocomposites by thermally conductive and electrically insulating boron nitride nanotubes. *ACS Appl. Nano Mater.* **3**, 364–374 (2020)
 21. J. Guan, B. Ashrafi, Y. Martinez-Rubi, M.B. Jakubinek, M. Rahmat, K.S. Kim, B. Simard, Epoxy resin nanocomposites with hydroxyl (OH) and amino (NH₂) functionalized boron nitride nanotubes. *Nanocomposites* **4**, 10–7 (2018)
 22. C. Zhi, Y. Bando, T. Terao, C. Tang, H. Kuwahara, D. Golberg, Towards thermoconductive, electrically insulating polymeric composites with boron nitride nanotubes as fillers. *Adv. Funct. Mater.* **19**, 1857–1862 (2009)
 23. H. Chang, M. Lu, P.J. Arias-Monje, J. Luo, C. Park, S. Kumar, Determining the orientation and interfacial stress transfer of boron nitride nanotube composite fibers for reinforced polymeric materials. *ACS Appl. Nano Mater.* **2**, 6670–6676 (2019)
 24. H. Chang, M. Lu, J. Luo, J.G. Park, R. Liang, C. Park, S. Kumar, Polyacrylonitrile/boron nitride nanotubes composite precursor and carbon fibers. *Carbon* **147**, 419–426 (2019)
 25. M.T. Byrne, Y.K. Gun'ko, Recent advances in research on carbon nanotube-polymer composites. *Adv. Mater.* **22**, 1672–88 (2010)
 26. O.Q. Alsmairat, F. Gou, C.M. Dmuchowski, P.R. Chiarot, C. Park, R.N. Miles, C. Ke, Quantifying the interfacial load transfer in electrospun carbon nanotube polymer nanocomposite microfibers by using in situ Raman micromechanical characterization techniques. *J. Phys. D* **53**, 365302 (2020)
 27. R. Arenal, A.C. Ferrari, S. Reich, L. Wirtz, J.Y. Mevellec, S. Lefrant, A. Rubio, A. Loiseau, Raman spectroscopy of single-wall boron nitride nanotubes. *Nano Lett.* **6**, 1812–1816 (2006)
 28. R.J. Nemanich, S.A. Solin, R.M. Martin, Light scattering study of boron nitride microcrystals. *Phys. Rev. B* **23**, 6348–6356 (1981)
 29. H.H. Gommans, J.W. Alldredge, H. Tashiro, J. Park, J. Magnuson, A.G. Rinzler, Fibers of aligned single-walled carbon nanotubes: polarized Raman spectroscopy. *J. Appl. Phys.* **88**, 2509–2514 (2000)
 30. K.R. Jiang, L.S. Penn, Improved analysis and experimental evaluation of the single filament pull-out test. *Compos. Sci. Technol.* **45**, 89–103 (1992)
 31. J. Zeng, B. Saltysiak, W.S. Johnson, D.A. Schiraldi, S. Kumar, Processing and properties of poly(methyl methacrylate)/carbon nano fiber composites. *Compos. B* **35**, 173–8 (2004)
 32. M. Loos, Fundamentals of polymer matrix composites containing CNTs, in *CNR Polymer Science and Technology*. (William Andrew Publishing, Norwich, 2015), pp. 125–70
 33. Z. Jia, Z. Wang, C. Xu, J. Liang, B. Wei, D. Wu, S. Zhu, Study on poly(methyl methacrylate)/carbon nanotube composites. *Mater. Sci. Eng. A* **271**, 395–400 (1999)
 34. M.W. Smith, K.C. Jordan, C. Park, J.-W. Kim, P.T. Lillehei, R. Crooks, J.S. Harrison, Very long single- and few-walled boron nitride nanotubes via the pressurized vapor/condenser method. *Nanotechnology* **20**, 505604 (2009)
 35. V. Yamakov, C. Park, J.H. Kang, X. Chen, C. Ke, C. Fay, Piezoelectric and elastic properties of multiwall boron-nitride nanotubes and their fibers: a molecular dynamics study. *Comput. Mater. Sci.* **135**, 29–42 (2017)